UC Davis
UC Davis Previously Published Works

Title
Membrane Dynamics at the Nuclear Exchange Junction during Early Mating (One to Four Hours) in the Ciliate Tetrahymena thermophila

Permalink
https://escholarship.org/uc/item/83f6f9zd

Journal
mSphere, 14(2)

ISSN
1556-6811

Authors
Cole, Eric S
Giddings, Thomas H
Ozzello, Courtney
et al.

Publication Date
2015-02-01

DOI
10.1128/ec.00164-14

Peer reviewed

Membrane Dynamics at the Nuclear Exchange Junction during Early Mating (One to Four Hours) in the Ciliate *Tetrahymena thermophila*

Eric S. Cole,[a] Thomas H. Giddings, Jr.,[b] Courtney Ozzello,[b] Mark Winey,[b] Eileen O'Toole,[c] Judy Orias,[d] Eileen Hamilton,[d] Sabrice Guerrier,[e] Anna Ballard,[a] Tyler Aronstein[a]

Biology Deparment, St. Olaf College, Northfield, Minnesota, USA[a]; Department of Molecular, Cellular, and Developmental Biology, University of Colorado, Boulder, Colorado, USA[b]; The Boulder Laboratory for 3D Electron Microscopy of Cells, Department of Molecular, Cellular, and Developmental Biology, University of Colorado, Boulder, Colorado, USA[c]; Department of Molecular, Cellular and Developmental Biology, University of California, Santa Barbara, California, USA[d]; Biology Department, Millsaps College, Jackson, Mississippi, USA[e]

Using serial-section transmission electron microscopy and three-dimensional (3D) electron tomography, we characterized membrane dynamics that accompany the construction of a nuclear exchange junction between mating cells in the ciliate *Tetrahymena thermophila*. Our methods revealed a number of previously unknown features. (i) Membrane fusion is initiated by the extension of hundreds of 50-nm-diameter protrusions from the plasma membrane. These protrusions extend from both mating cells across the intercellular space to fuse with membrane of the mating partner. (ii) During this process, small membrane-bound vesicles or tubules are shed from the plasma membrane and into the extracellular space within the junction. The resultant vesicle-filled pockets within the extracellular space are referred to as junction lumens. (iii) As junction lumens fill with extracellular microvesicles and swell, the plasma membrane limiting these swellings undergoes another deformation, pinching off vesicle-filled vacuoles into the cytoplasm (reclamation). (iv) These structures (resembling multivesicular bodies) seem to associate with autophagosomes abundant near the exchange junction. We propose a model characterizing the membrane-remodeling events that establish cytoplasmic continuity between mating *Tetrahymena* cells. We also discuss the possible role of nonvesicular lipid transport in conditioning the exchange junction lipid environment. Finally, we raise the possibility of an intercellular signaling mechanism involving microvesicle shedding and uptake.

Fertilization in most eukaryotic organisms involves whole-cell fusion and integration of haploid gametes into a single, diploid zygotic cell. Ciliates are unique in that fertilization involves formation of a transient region of membrane fusion that supports bilateral nuclear exchange. Following reciprocal nuclear exchange and fertilization, mating partners separate and reestablish cellular integrity rather than integrate into a single, zygotic whole. The process of cortical remodeling that supports this transient exchange of nuclear and cytoplasmic contents has received little attention since the early 1980s, when a series of elegant ultrastructural investigations were published (1–3). These historical studies revealed a dramatic landscape involving both membrane and cytoskeletal dynamics (reviewed in reference 4), yet many aspects of this cortical remodeling have remained virtually unexplored, and numerous features can now be reinterpreted in light of a more modern, 3-dimensional (3D) approach.

In the laboratory, mating can be initiated when cells of one mating type are subjected to nutritional deprivation and mixed with starved cells of a complementary mating type (5, 6). There are seven mating types in *Tetrahymena thermophila*, each capable of forming pairs with any of the other six (7). The process of mating type determination for *T. thermophila* was recently characterized in the laboratory of Eduardo Orias (8). The starvation interval is formally known as initiation (5). When starved cell lines of complementary mating types are mixed in equal numbers, an hour-long period of physical interaction is required to trigger formation of an adhesion zone at the cell's anterior (Fig. 1A to C). This period is known as costimulation (9, 10). Once formed, the cell adhesion zone becomes a theater for dynamic membrane remodeling. Starting 1.5 h after mixing (all time points refer to experiments conducted at 30°C), hundreds of membrane fusion events are initi-

ated within the adhesion zone between mating partners at individual plasma membrane foci (1). These pores, initially reported as 100 nm in diameter or less, enlarge until the expansion front of one pore encounters the expansion front of a neighboring pore (Fig. 1). At these contact fronts, the residual membrane resolves into a network of interconnecting membrane tubules (Fig. 1F to H) 90 nm in diameter, as revealed by high-voltage electron microscopy (2). It is through this "membrane curtain" that gametic pronuclei are driven by a mesh or basket of short, crisscrossing microtubules (2). Subsequent to pronuclear exchange, the dual plasma membranes are restored and exconjugants separate, 12 h after cells were initially mixed.

Though these early studies reveal broad strokes involved in creating the nuclear exchange junction, they raise numerous mechanistic questions. (i) How are membrane pores initiated? (ii) How do these pores (initially 100 nm across) expand to accom-

FIG 1 A schematic diagram showing the process of pair formation in mating *Tetrahymena thermophila* (A to D) and the accompanying modifications (E to H) of the nuclear exchange junction shown *en face* (central gray images) and in (rightmost images) as most of our TEM sections were oriented. (A) Costimulated cells form specialized tips. (B) Modified tips come into contact and adhere. (C and E) A broad adhesion zone develops, holding mating partners together and permitting membrane fusion events to occur, transforming loose pairs into tight pairs. (D) A mating pair that has been disrupted to reveal the exchange junction full of hundreds of fusion pores. (E to H) *En face* and cross-sectional representations of the adhesion zone prior to and during pore formation. (F) The exchange junction after membrane fusion events have created hundreds of small (0.1-μm-diameter) pores (5 pores are shown in the cross-sectional representation). (G) The same junction after pore expansion has enlarged the pores. (H) After pore expansion fronts collide, the residual membrane is transformed into a network or curtain of membrane tubules (90 nm in diameter).

modate the passage of a 3-μm-diameter migratory pronucleus? (iii) What changes must occur in the phospholipid environment of the exchange junction to support the topological transition from laminar sheets to a network of 90-nm-diameter tubules? (iv) How do mating cells restore membrane integrity after nuclear exchange? Using a 3D ultrastructural approach, we confirmed and extended previous observations and identified novel features within the nuclear exchange junction illuminating a dynamic cortical landscape. This study allowed us to formulate hypotheses regarding the mechanism behind these membrane dynamics and provide a benchmark for comparison with mutant strains, setting the stage for future investigations.

MATERIALS AND METHODS

Cell culture. Cells were grown in a proteose peptone growth medium supplemented with iron chloride (11). Cells of complementary mating types were starved; cultures were centrifuged and transferred to 10 mM Tris, pH 7.4 (two rinses). After 12 to 18 h of starvation, mating types were mixed at equal densities (in the range from 2×10^5 to 8×10^5 cells/ml) in 100-mm petri dishes (10-ml total volume). At appropriate times after mixing, samples were harvested and fixed for transmission electron microscopy (TEM).

Conventional preparation for thin-section TEM (chemical fixation). Mating cells (pairing cultures confirmed by light microscopy) were sampled at various times. Approximately 10^5 to 10^6 mating pairs were pelleted by gentle centrifugation (setting 4 on an IEC clinical desktop centrifuge [Thermo Scientific], approximately $300 \times g$). An equal volume of cells plus medium was mixed with double-strength fixative (double

strength = 5% glutaraldehyde in 0.2 M sodium cacodylate, pH 7.2). Cells were fixed for 1 h at room temperature. Cells were then spun into a loose pellet, and the supernatant was discarded. The pellet was placed on ice and given three 10-min rinses in buffer (0.1 M sodium cacodylate, pH 7.2). The final supernatant was discarded. Cells were fixed for 1 h at room temperature in 2% osmium tetroxide (4% stock osmium diluted in 0.1 M sodium cacodylate, pH 7.2). Cells were then spun into a loose pellet and the supernatant was discarded. The cell pellet was placed on ice and given two 10-min rinses with buffer (0.1 M sodium cacodylate, pH 7.2). Cells were pelleted and the supernatant was discarded. The pellet was rinsed once for 5 min with ice-cold distilled water. Cells were then pelleted, and the supernatant was discarded. The resultant pellet was soaked 20 min in ice-cold 1% aqueous uranyl acetate. Cells were pelleted again and rinsed once for 5 min with ice-cold distilled water. Cells were then placed on ice and dehydrated using a graded ethanol series (10, 30, 50, and 70%); each treatment was for 10 min. The resultant pellet was transferred to 90% ethanol for 10 min at room temperature and then twice to 100% ethanol for 15 min at room temperature. The dehydrated pellet was infiltrated in Spurr's medium. For the final 4-h Spurr soak, pelleted material was transferred to Beem capsules, fresh Spurr's medium was added, and mating cells were spun to the bottom of the capsule. Samples were left to sit for 4 h and polymerized overnight at 65 to 70°C. Cells were sectioned and placed on Formvar-coated grids. Sections were stained for 20 min with uranyl acetate and then for 7 min in lead citrate (12).

Freeze-substitution TEM. Cultures with mating pairs of *Tetrahymena* were prepared for transmission electron microscopy as described in references 13 and 14. Briefly, cells were harvested by centrifugation into a cryoprotectant solution consisting of 15% dextran (9-11KD; Sigma) and 5% bovine serum albumin (BSA) in 10 mM Tris and frozen in a Wohlwend Compact 02 high-pressure freezer. Samples were freeze-substituted in 2% osmium tetroxide–0.1% uranyl acetate in acetone and embedded in Spurr's epoxy resin. Serial thin sections were poststained with uranyl acetate and lead citrate and then imaged in a Philips CM100 TEM.

Tomography. Electron tomography of *Tetrahymena* was performed as described previously (14). Briefly, serial thick (250-nm) sections were collected onto Formvar-coated slot grids and stained with 2% uranyl acetate and Reynold's lead citrate. Gold particles (15 nm) were affixed to the sections for use as alignment markers. Tomography was carried out using a TECHNAI F20 or F30 electron microscope (FEI Corp., Hillsboro, OR) using the SerialEM image acquisition program (15). Dual-axis tilt series were collected every 1° over a ±60° range using a Gatan 2kx2k charge-coupled-device (CCD) camera at a pixel size of 1.2 to 1.5 nm. The tilt series were aligned and tomograms computed and modeled using the IMOD software package (16, 17). In total, seven tomograms were computed: five for events occurring during pore formation leading up to nuclear selection (approximately 2 to 4 h after mixing), one for a pair in which the migratory pronucleus is docked at the junction (approximately 5 h after mixing), and one for a pair in which the pronucleus has just been delivered across the mating junction (approximately 5.5 h). Cellular features were modeled and color-coded as follows: microtubules, red; plasma membrane, bright green; transjunctional reticulum (TJR; possibly smooth endoplasmic reticulum [SER]), pale blue; nuclear envelope, dark blue; autophagosomes, purple; mucocyst limiting membrane, dark green; mucocyst contents, brown; and lipid droplets, yellow. These features were manually traced in the volumes, and projections of the 3D models were displayed and rotated to study the 3D geometry.

RESULTS

Cell adhesion. Early during pair formation (1 to 1.5 h), mating cells attach to one another at a specialized cortical region anterior to the oral apparatus (Fig. 1B and C). This initial domain of contact (the adhesion zone) is approximately 8 to 10 μm in diameter and shaped like an inverted heart (Fig. 1; central gray images depict junction *en face*). Transmission electron microscopy (TEM) revealed that the two plasma membranes, one from each partner,
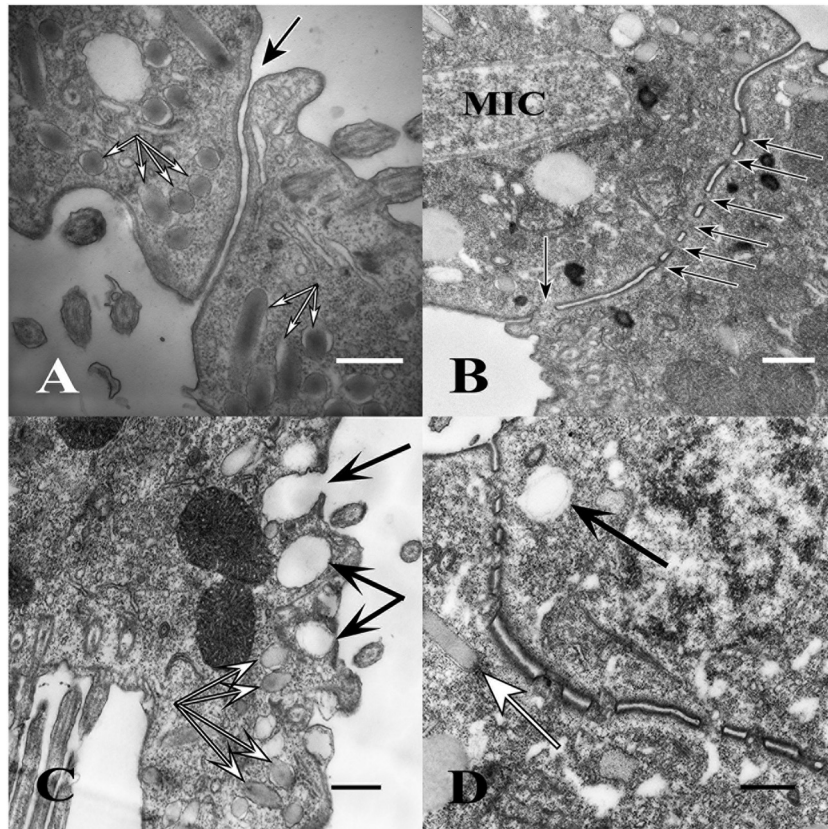
FIG 2 Thin-section (80 nm) TEM images (chemical fixation) showing an early exchange junction. (A) Before pore formation during cell adhesion. The black arrow indicates where the junction cleft is in continuity with the extracellular space. White arrows indicate dense core secretory granules that have not yet discharged their contents via exocytosis. (B) Exchange junction showing completed exchange junction pores (black arrows) and elongated prophase 1 micronucleus (MIC). (C) Docked and discharged mucocysts in the vicinity of the exchange junction. Black arrows indicate mucocysts that have discharged their contents. White arrows indicate undischarged mucocysts. (D) Discharged, internalized mucocyst membrane (black arrow) and undischarged mucocyst (white arrow) near the exchange junction. Scale bars = 500 nm.

press together with a uniform 40- to 50-nm gap (Fig. 2A) of extracellular space between them (illustrated as parallel lines in Fig. 1E, depicting a cross-sectional view). The region of extracellular space trapped between the two closely apposed membranes we have named the junction cleft. The cytoplasmic face of each membrane flanking the junction cleft is decorated by an electron-dense layer we refer to as the junction scaffold. Applying high-pressure freezing followed by freeze-substitution (rather than conventional chemical fixation), we generated unusually detailed images of the junction (Fig. 3). Using this technique, the junction cleft (not including the plasma membranes that define its borders) was measured at 33 to 44 nm across. The electron-dense scaffold decorating the cytoplasmic face of each plasma membrane exhibits a uniform 39-nm width appearing in micrographs as a pair of irregular, continuous lines parallel to the plasma membrane (Fig. 3A, white arrows) and anchored to it by short (33 to 39 nm) cross-struts spaced roughly 23 nm apart. In regions associated with pore formation, the scaffold appears to break down, creating discontinuities (Fig. 3B, white bracket).

Dense core secretory granules (mucocysts). Secretory granules were frequently found docked at the cell cortex in the immediate vicinity of the exchange junction, though never at the exchange junction membrane itself (Fig. 2A, white arrows). We also encountered secretory granules in the process of discharging

(Fig. 2C, black arrows). The limiting membranes of these dense core secretory granules do not appear to integrate into the plasma membrane after exocytosis (as previously proposed) but reseal, and the discharged mucocysts migrate as large, empty vacuoles back into the cytoplasm in a form of "kiss and run" exocytosis (18). Discharged mucocysts are readily identified by their size and lightly stained inner envelope, a residue of the discharged mucocyst contents, within an otherwise empty vacuolar membrane (Fig. 2C and D, black arrows). 3D electron tomography (ET) allowed us to trace membrane continuities within the cytoplasmic volume and between various organelles at 4- to 6-nm resolution and in 3D. Following exocytosis, we saw that the outer membrane of discharged granules becomes contiguous with a membrane reticulum in the cytoplasm (Fig. 4D to H). We traced this reticulum using electron tomography and found it contiguous with the transjunction reticulum, a membrane system that infiltrates expanding pores within the developing exchange junction complex (see below).

Pore initiation (membrane tubulation). Pairs fixed and examined 1.5 h after mixing (30°C) revealed mating junctions that were devoid of fusion pores (Fig. 2A). By 2 h, pores became abundant (Fig. 2B, arrows). After screening numerous samples of 1.5-h pairs, we found loosely bound pairs exhibiting the very earliest stages of pore formation; Fig. 3C shows a specimen prepared via chemical fixation. This example is noteworthy for two reasons.
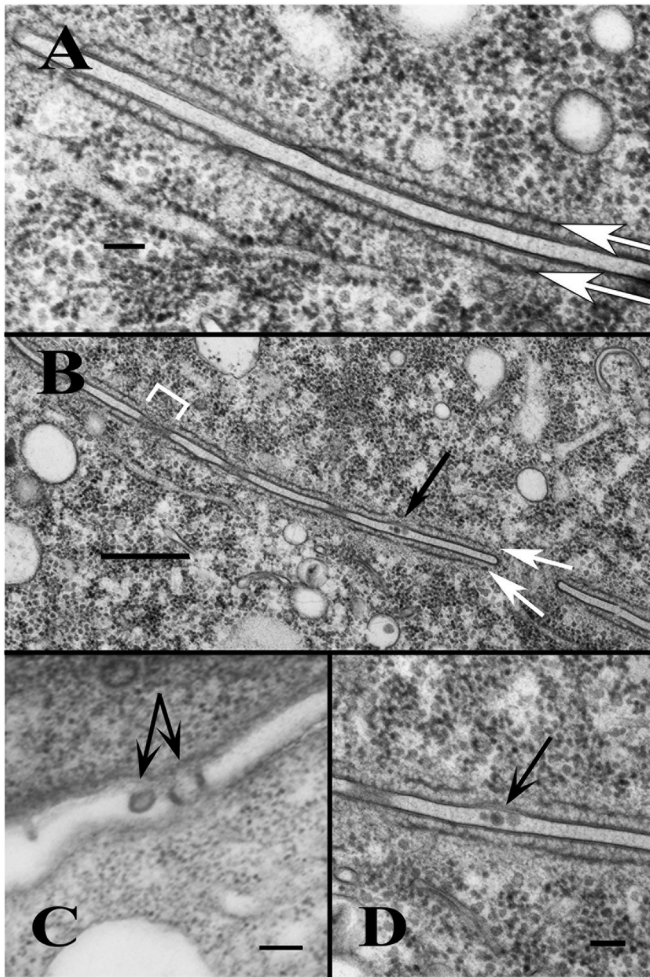
FIG 3 Freeze-substitution TEM showing nuclear exchange junction with well-preserved membrane and cytoskeletal components. (A) Arrows indicate the junction scaffold, a proteinaceous layer closely apposed to the cytoplasmic face of each cell's plasma membrane. Cross-struts are visible connecting the scaffold to the membrane. Scale bar = 100 nm. (B) Low-magnification image showing scaffold (white arrows), localized thinning of the scaffold near junction pores (white bracket), and membrane protuberances (black arrows, magnified in panel D). Scale bar = 500 nm. (C) At 1.5 h into costimulation, a mating pair with one point of physical contact. Arrows indicate membrane protrusions extending from upper cell and across the junction cleft. Scale bars = 100 nm. (D) Magnified view of protuberances in panel B. Scale = 100 nm.

There are protuberances emanating from the upper cell partner. The leftmost protuberance is a 50-nm tubule (inner diameter) with a densely staining cytoplasmic lining to the membrane (left arrow). The adjacent, rightmost structure appears to be a similar protuberance whose membrane has fused with the plasma membrane of the apposing cell (right arrow). The densely stained material is now concentrated on the lateral flanks of this cytoplasmic bridge. The resultant pore is approximately 80 nm in diameter. Once identified, these structures were noted to appear with fair frequency (Fig. 3B and D, black arrows; see also Fig. S1 and S2 in the supplemental material). A consistent feature of early exchange junction pores is an electron-dense material forming a cupped lining to the cytoplasmic channels (Fig. 2B and D). By 2 h, pore initiation at the mating junction appears largely complete.

Junction lumens and extracellular microvesicles. In numer-

ous thin sections, we encountered membrane-bound structures within the junction cleft. These were sites where the exchange junction membrane had ballooned around a cavity of extracellular space, forming large (200- to 300-nm diameter) chambers or blisters whose lumens were contiguous with the extracellular space of the junction cleft. These junction lumens were consistently occupied by collections of small, irregularly shaped, membrane-bound vesicles or tubules (Fig. 5). The average dimensions of the intraluminal vesicles were 34.3 nm (standard error, ±3.9) by 54.0 nm (±6.6) (n = 18). These membrane-bound vesicles resemble the variously named ectosomes, shedding microvesicles, or extracellular microvesicles (EMVs) described for other systems (19–21). Serial section through six individual junction lumens revealed that each structure formed immediately adjacent to one or more of the completed pores with the margin of the pore forming one wall of the junction lumen (see Fig. S1 and S2 in the supplemental material). The dimensions of these extracellular microvesicles were similar to those of the protuberances associated with initial pore formation.

A second class of membrane deformations was observed in association with what appeared to be reclamation of the contents of the junction lumens. In such cases, thin (18-nm) folds of plasma membrane protruded into the junction lumen (Fig. 5G to I). 3D electron tomography revealed these to be broad folds of membrane (dissimilar from the earlier membrane protuberances) that appear to delimit the contents of the junction lumen (Fig. 6). In the same area, we found objects resembling multivesicular bodies (MVBs). These we interpreted as collections of luminal vesicles that had been delimited by membrane folds and had pinched off from the exchange junction and internalized within the cytoplasm. In some cases, these MVB-like structures appeared to be enclosed within a double-walled membrane capsule resembling classic autophagosomes (Fig. 5L, bracket). These are described in greater detail below.

Autophagosomes and MVBs. Thin-section TEM revealed a substantial number of double-membrane circular and "C"-shaped profiles near the exchange junction (Fig. 5J to L). From the ultrastructure literature, these are recognizable as autophagosomes in various stages of development (22–25). Autophagosomes have been identified at the exchange junction of mating *Tetrahymena* cells from studies employing the fluorescent probe monodansyl cadaverine in which they have been implicated in programmed nuclear degeneration (24). Also within the cytoplasm, and in the vicinity of the mating junction, we identified what appeared to be conventional MVBs in close association with the double-walled cups or vacuoles that fit the description of autophagosomes (Fig. 5K and L). It was usually not possible to tell whether the previously described vesicle-filled junction lumens were in some way related to the conventional MVBs located in the cytoplasm. In one particular tomogram, however, we observed the membrane limiting a junction lumen protruding directly into the interior of an adjacent double-walled structure (Fig. 6D to F). This example is also notable in that microvesicles were being shed from one mating partner, while the luminal membrane appeared to be extending into the cytoplasm of the other mating partner and into a nearby autophagosome. This raises the possibility of microvesicle-mediated transport across the cleft and between mating cells.

Infiltration of a membrane reticulum (the transjunction reticulum [TJR]) across developing intercellular pores. Once the cytoplasm of mating pairs becomes contiguous through the estab-
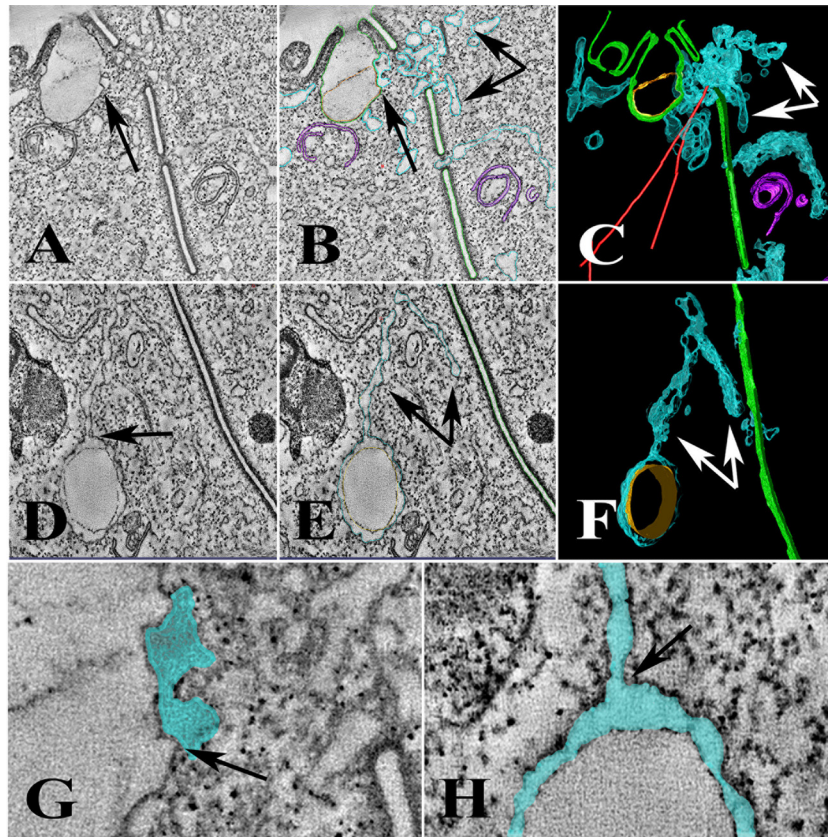
FIG 4 Tomography of discharged mucocysts near exchange junction. Top panels show a mucocyst discharging its contents at the plasma membrane, adjacent to the junction cleft. (A) The black arrow indicates association between limiting membrane of the mucocyst and transjunction reticulum (TJR) that also infiltrates exchange junction pores. (B and C) Same image showing progressive modeling. Green, plasma membrane and mucocyst membrane that is transiently continuous with it; turquoise, TJR (white arrows); red, microtubules; purple, autophagosomes; brown, residue within the discharged mucocyst lumen. The region at the arrow in panel A is magnified in panel G, showing tight apposition but no continuity between the mucocyst membrane and the TJR. (D) Discharged, recycled mucocyst near junction showing continuity between the limiting membrane of the mucocyst and the TJR. (E and F) Same image showing progressive modeling. Arrows indicate contiguous membrane reticulum stretching from mucocyst toward exchange junction pore. The region indicated by the arrow in panel D is magnified in Fig. 3H, showing continuity of mucocyst lumen and lumen of the TJR.

lishment of hundreds of intercellular pores, these pores become occluded with a "filamentous or membranous material" (1). Thin sections, particularly of early pairs (2.5 to 4.0 h), reveal that the pores are occupied by faintly staining membranous lobes. It was only after we started deploying thick sections and performing 3D electron tomography that we began to appreciate the extent of this membrane system and its continuity with other, more easily identified membrane compartments (Fig. 7). With tomography, the lobes apparent in our thin-section work were revealed to be branches of an extensive, interconnected membrane reticulum reaching into the cytoplasm of each partner. The lightly stained membrane of these lobes comes into close physical proximity with the densely stained plasma membrane lining the pores. We measured the gap separating reticulum from pore walls as close as 10 to 20 nm.

By modeling tomograms generated from exchange junction material, we were able to trace the trajectory of this intrapore reticulum and establish its continuity with other membrane systems. This TJR was seen to connect with the membrane of discharged dense core secretory granules or mucocysts, though it was never seen in contact with the limiting membrane of docked secretory granules until after they had discharged their contents via

exocytosis (Fig. 4). The transjunction reticulum also came into intimate contact with the surfaces of lipid droplets (Fig. 7). Finally, we observed continuity of the transjunction reticulum with the outer membrane of the nuclear envelope (Fig. 8). In 3 instances, we traced a continuous membrane from the nuclear envelope into the highly branched reticulum that infiltrated the junction pores. We conclude that this material was smooth endoplasmic reticulum (SER) by virtue of both its characteristic pale staining and its continuity with the outer nuclear envelope. Later in development, when the postmeiotic nuclei became pressed against the nuclear exchange junction prior to exchange (4 to 4.5 h), the TJR disappeared, and pores were filled with a fine, filamentous material (Fig. 9 see also Movies S3 and S4 in the supplemental material). These filaments were typically 12 to 15 nm in diameter and persisted within the junction pores even after nuclear exchange.

DISCUSSION

Conjugation in the ciliate *Tetrahymena thermophila* provides a unique, inducible program of membrane and cytoskeletal remodeling that first forms a junction between mating cells, then transforms this dual-membrane into a curtain through which nuclei may pass, and, finally, restores membrane integrity of the individ-
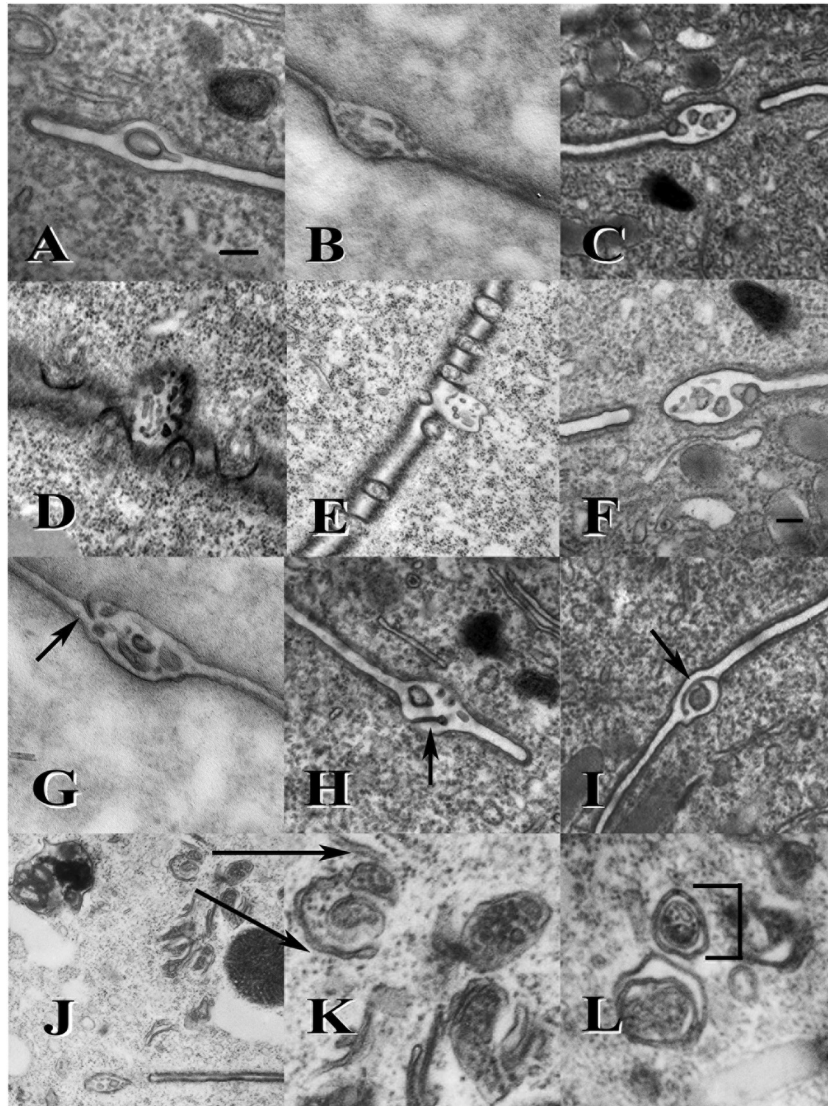
FIG 5 TEM gallery (chemical fixation) of junction lumens filled with microvesicles. Panels A to F show swellings of the extracellular space within the junction cleft. Most are shown in close proximity to one or more pore margins, each filled with irregular shaped vesicles or tubules budding off from the plasma membrane. Panels G to I show a 2nd kind of membrane egression (arrows). A tightly compressed membrane fold appears to be delimiting contents of a junction lumen into a diverticulum that sequesters these materials into the. Panels J and K show multivesicular bodies (MVBs) in the vicinity of the exchange junction where junction lumens are actively being formed (arrows). MVBs are seen near double-membrane compartments resembling autophagosomes. Panel L shows autophagosome (brackets) encompassing an MVB (also in proximity to the exchange junction, not shown).

ual exconjugants. Wolfe (1) provided a detailed description of the process of pore formation employing both thin-section TEM and freeze-fracture scanning electron microscopy (SEM) techniques. He described a cortical field supporting hundreds of individual membrane-fusion events that create a perforated plate. Orias et al. (2) explored subsequent events that transform this perforated plate into a curtain of membrane tubules as well as a unique microtubule meshwork that propels gametic pronuclei across this membrane curtain in a process of bilateral nuclear exchange. Now, 30 years later, we have revisited this intercellular theater using serial-section TEM, flash-freezing, and 3D electron tomography. In particular, we sought ultrastructural details that might provide insight into (i) how the membrane pores are initiated, (ii) how a series of 100-nm pores expand to accommodate the passage

of a 3-μm-diameter pronucleus, and (iii) what changes must occur in the lipid environment at the exchange junction to support the topological transition from laminar sheets to a network of 90-nm-diameter tubules.

From cell adhesion to membrane fusion. Gamete interactions can be divided into three processes: gamete recognition, cell adhesion, and cell fusion. Ciliate conjugation can be viewed in a similar way. Costimulation (a 1-h period of cell-cell interaction between starved, sexually compatible mating types) is necessary for the promotion of pair formation. During this stage, some form of mating-type recognition must be involved, as mixing same-sex cells does not lead to cell adhesion. Costimulation leads to weak, nonspecific cell-cell adhesions that form even between cells of the same mating type (26). Costimulation also leads to a type of apical
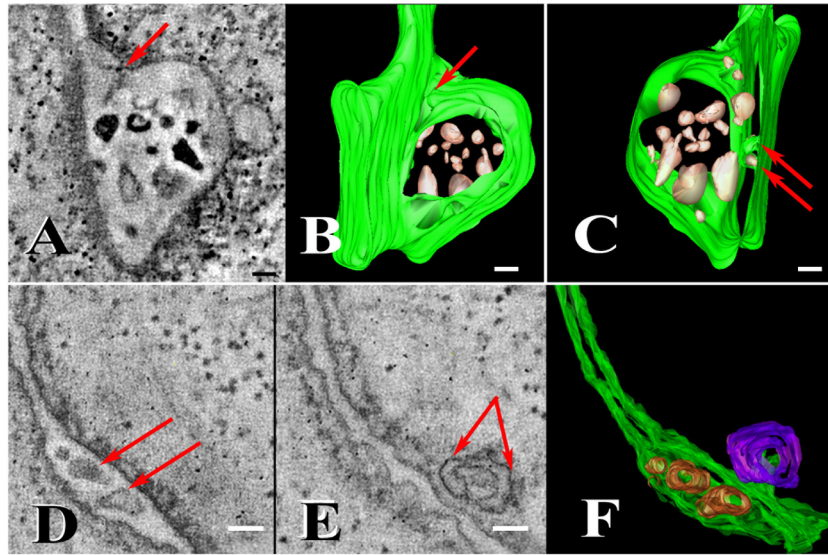
FIG 6 Electron tomography showing egression and pinching off of a vesicle-filled vacuole from the junction cleft. (A) Optical section from original tomogram showing a vesicle-filled junction lumen and a site of membrane egression from the cytoplasm (arrow). (B) Model generated from full 3D tomogram (see below). Green shows the plasma membrane of junction and junction lumen. Gold highlights internal vesicles. The arrow indicates a cleft where the plasma membrane appears to be pinching into extracellular space of the lumen. (C) Model optically rotated to view from "below." Arrows indicate continuing process of membrane protuberance into the junction cleft contiguous with the junction lumen. This model allowed us to see membrane budding from the junction lumen and into the lumen of a developing autophagosome. Scale bars for panels A to C = 50 nm. (D to F) Electron tomogram showing an autophagosome forming directly around a membrane diverticulum as it buds off a vesicle-filled junction lumen. Panel D shows the small junction lumen with several shed microvesicles (arrows). Panel B shows the same region of exchange junction as in panel D imaged deeper in the section, showing a double-walled autophagophore in close association with the junction membrane. Green, plasma membrane; gold, membrane of extracellular, shed microvesicles; purple, autophagosome membrane. Scale bars for panels D to F = 100 nm.

"capping" involving highly mobile surface glycoproteins that bind to the plant lectin concanavalin A (ConA) (27). ConA-binding proteins form a plaque over the mating surface at the anterior end of the cell. Mating cultures incubated in the presence of ConA are inhibited from forming pairs, suggesting that these surface glycoproteins are necessary for cell adhesion (28, 29). After the initial round of nonspecific cell adhesion, homotypic pairs dissociate, whereas heterotypic pairs are transformed into strongly bonded partners. This represents a second aspect of mating-type recognition. It is likely that the mating-type recognition involved in both triggering costimulation and stabilizing heterotypic pairs involves proteins encoded by the *Tetrahymena* mating-type locus, recently identified and characterized by Cervantes et al. (8). Once cell adhesion is established and heterotypic mating partners have been stabilized, the stage is set for membrane fusion. Hundreds of membrane fusion events transform the weakly bound pairs into tightly bound pairs. Our study provides the first images of the membrane events that immediately precede fusion and pore formation. We characterize a period of membrane protrusion in which small (50-nm) protuberances extend from one cell into the junction cleft and toward the partner's surface. These are reminiscent of the fertilization tubules that extend from the plus gamete of *Chlamydomonas* toward the minus gamete during mating (30). A striking difference is that in the algae, only one fertilization tubule is expressed and only from one of the mating partners, whereas in *Tetrahymena*, there are hundreds of protrusions, and they are expressed from both partners. A homolog to a highly conserved, male gamete-specific fusogen (Hap2p) has recently been implicated in bringing about these membrane fusion events during mating in both *Chlamydomonas* (31) and *Tetrahymena* (32).

Pore expansion: a model for membrane conditioning. Historical accounts have noted that exchange junction pores become occluded with some membranous or filamentous material (1). Modeling electron tomograms from thick sections of early exchange junction material allowed us to characterize this occluding material, revealing it to be an extensive membrane reticulum, quite likely an extension of the SER. Several things are notable. First, within early pairs, this transjunction reticulum is a ubiquitous structure occupying every single pore. Second, the membrane of this reticulum comes into intimate proximity (10 to 20 nm) with the membrane of the pore margins. Third, we have traced the reticulum and found it to come into close proximity with lipid droplets and to be physically contiguous with the membranes of other organelles, including the outer nuclear envelope and the limiting membrane of discharged secretory granules. Finally, the transjunction reticulum of one cell traverses the pore, establishing continuity with a similar membrane system in the mating partner. This system resembles the membrane architecture of the plant cell plasmodesmata, a stable pore that connects the cytoplasm of adjacent cells. Endoplasmic reticulum (ER) from each plant cell is connected via the desmotubule, a specialized region of the ER that traverses this intercellular junction (33, 34). It is also interesting that in plants, lipid bodies have been found in intimate association with the ER, where they may "usurp membranous material, possibly from ER strands that are continuous with the desmotubule in the center of the PD channel" (35). From the animal kingdom, the transjunction reticulum is reminiscent of the fusome, a specialized region of ER that connects nurse cells through the ring canal during *Drosophila* embryogenesis (36).
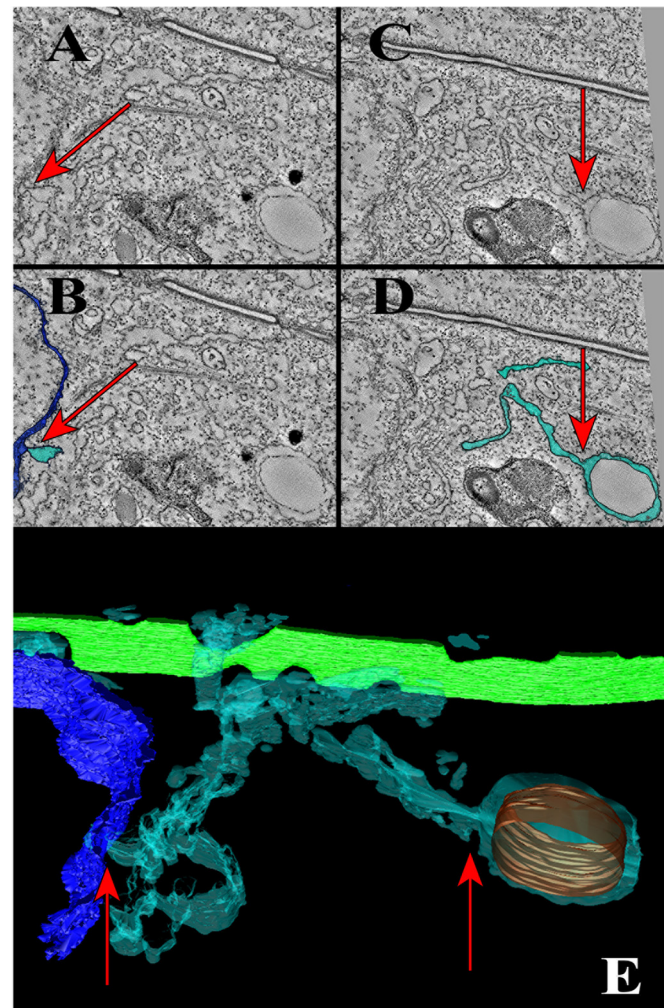
In *Tetrahymena*, the ubiquity of this membrane system in tight association with the margins of every junction pore examined
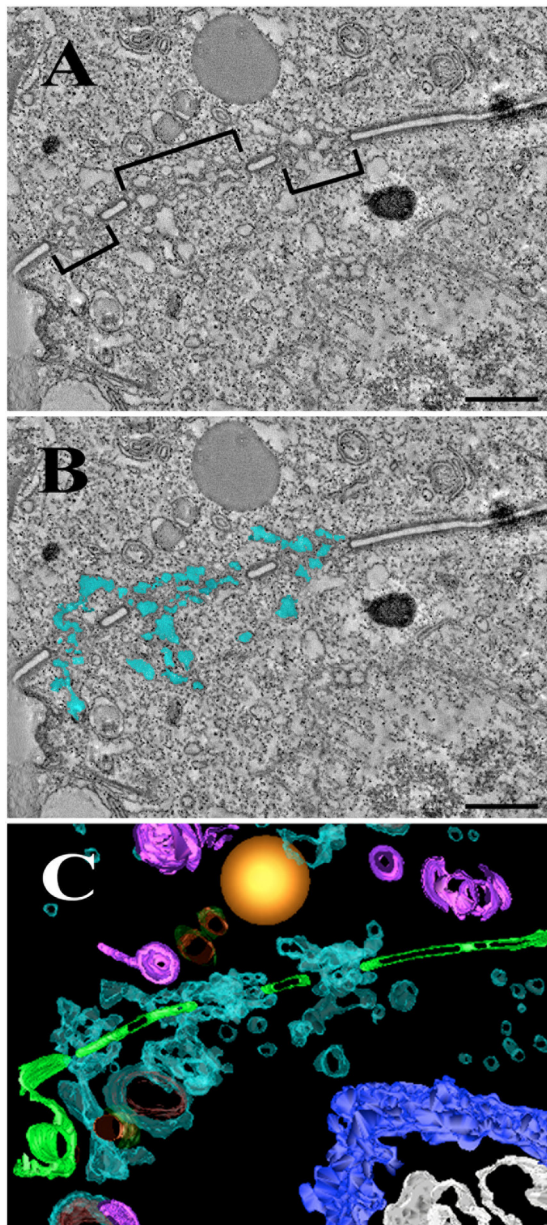
FIG 7 Electron tomography highlighting the transjunction reticulum (TJR) infiltrating the junction pores. (A) Initial tomogram section through the exchange junction. Brackets indicate pores. (B) Same section as in panel A, with transjunction reticulum colored turquoise. Scale bars = 500 nm. (C) 3D model of same region showing the plasma membrane (green), the transjunction reticulum (turquoise), lipid droplet (gold), autophagosome membranes (purple), nuclear envelope (blue), and chromatin (gray). Mucocyst outer membranes are dark green, and their contents are brown. (For a 3D model of this, see Movie S1 in the supplemental material.)

FIG 8 Electron tomography highlighting the continuity of the transjunction reticulum (TJR) with nuclear envelope and the limiting membrane of a discharged secretory granule. (A) Initial tomogram section through the exchange junction. The arrow indicates the point of continuity between the TJR and nuclear envelope. (B) Same section as in panel A, with the TJR colored turquoise and nuclear envelope dark blue. (C) Same specimen showing a deeper section, highlighting the limiting membrane of a discharged mucocyst. The arrow indicates the point of continuity with the TJR. (D) Same view, with membranes colored turquoise. (E) Composite 3D model of same region showing both discharged mucocyst (right arrow) and contact with nuclear envelope (left arrow). The plasma membrane of the exchange junction is colored green, the TJR turquoise, and the nuclear envelope blue. Secretory granule contents are brown. (For a 3D model of this, see Movie S2 in the supplemental material.)
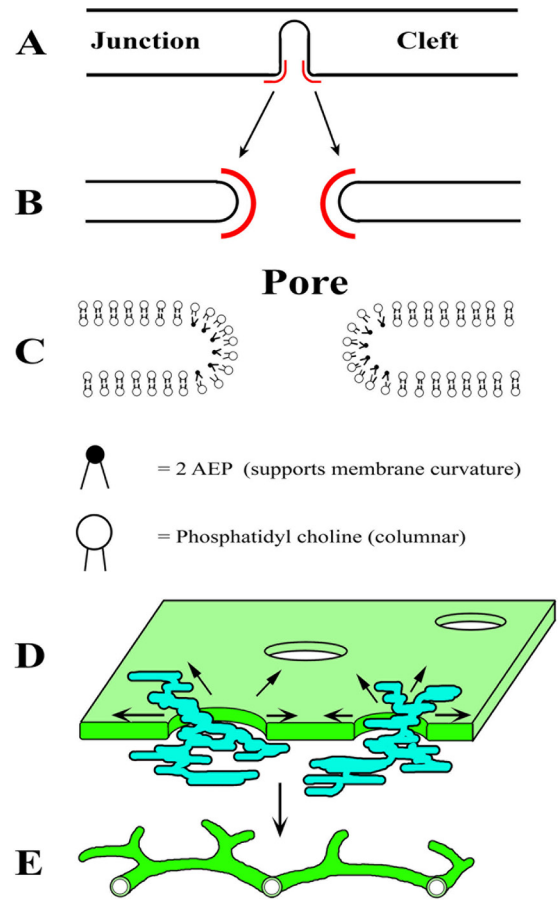
argues for some critical role. What membrane dynamics are active during this period of development? First, pores are expanding. During the initial 4 h of mating, pore diameters expand by up to an order of magnitude ([1]). This represents a loss of approximately 1.0 μm^2 of membrane surface per pore when both partners' surfaces are considered. It should be noted that only about 20% of pores expand to this extent; most pores show only a 5- to 6-fold expansion in diameter during this time. This still represents a total

difference of approximately 100 μm^2 of membrane across the exchange junction. The difference in membrane surface area between early and later junctions could be accounted for in two ways. As expanding pores "collide," the resultant tubular curtain could be thrown into convoluted, 3-dimensional folds. One could then account for "missing" membrane on purely topological grounds. Alternatively, there could be a mechanism for excavating membrane from the expanding pore margins (see below). We never observed physical continuity between the transjunction reticulum and the plasma membrane (despite finding numerous instances of continuity with the nuclear envelope, a fairly rare
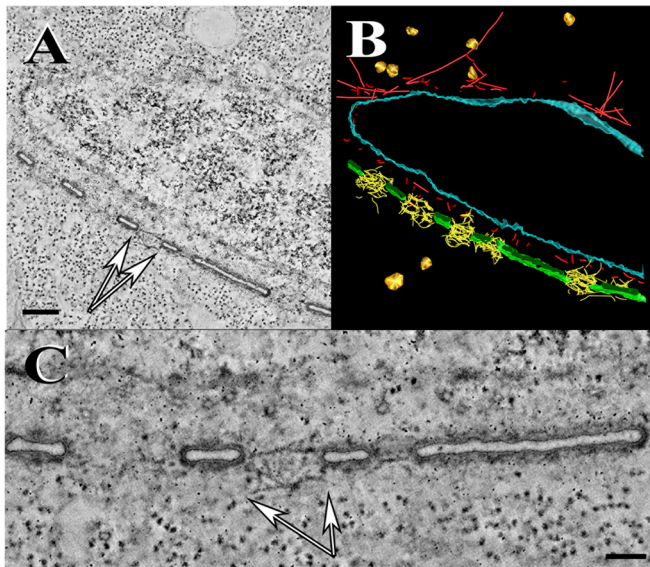
FIG 9 Electron tomography of a pre-exchange mating pair. The postmeiotic nucleus is docked at the exchange junction. (A) An optical section from the initial tomogram showing a nucleus docked at a junction with pores. White arrows indicate filaments (not membrane) occluding a pore (region is magnified in panel C). Scale bar = 250 nm. (B) Same region modeled in 3D with nuclear envelope (blue), plasma membrane (green), microtubules (red), intracellular vesicles (gold), and fine, 12- to 15-nm filaments (yellow). (C) Close-up of tomogram from panel A showing fine filaments (white arrows). Scale bar = 100 nm. This tomogram appears as a 3D model in Movies S3 and S4 in the supplemental material.

FIG 10 A model detailing membrane conditioning during pore expansion. (A) A membrane protrusion everts into extracellular junction cleft creating regions of tight curvature (highlighted in red). (B) After membrane fusion, the margins of a pore represent regions of tight curvature (red). (C) Asymmetric distribution of conical phospholipids such as 2-AEP within the extracellular leaf of a bilayer could help support tight curvature at the pores. (Panels B and C are modeled after the work of Kurczy et al. [38].) (D) Pores within the nuclear exchange junction are infiltrated with the transjunction reticulum (turquoise). As pores expand (black arrows), the TJR could supply specialized phospholipids (2-AEP) through nonvesicular lipid transfer. (E) Resulting network of membrane tubules once pore expansion fronts collide and merge.

occurrence itself). We also never observed anything resembling "blebbing" of vesicles from the plasma membrane toward the cytoplasm or fusion of vesicles with the TJR (though we saw large-vacuole reclamation not associated with the TJR). This argues against the TJR playing a direct role in membrane reclamation from the margins of expanding pores.

There are other membrane dynamics at play at this stage in development. Previous studies demonstrated replacement of cylindrical lipid species at the exchange junction with nonlamellar species that can support tight curvature during conjugation (37, 38). The margins of exchange junction pores and, later, the tubular curtain they transform into represent expanding regions of tight membrane curvature. As pores expand, and if lipid composition is critical to the establishment and maintenance of tight membrane curvature, then cells must replace columnar lipid species with nonlamellar species, and these must be preferentially shuttled from the cytoplasmic face (where they are presumably delivered) to the extracellular face of this positively curving (away from the cytoplasm) membrane (Fig. 10). Studies have uncovered mechanisms for nonvesicular lipid transport which allow lipid exchange or transfer from one membrane-bound compartment to another (39). Gene products such as phospholipid transfer proteins (PLTP) can operate over distances of 10 to 20 nm, the effective gap between the transjunction reticulum and the pore margin, making this a potential candidate for a mechanism of lipid exchange with the cytoplasmic leaf of the expanding pore membrane. It may be relevant that a *Tetrahymena* homolog to a PLTP (TTHERM_00052410) shows peak transcriptional activity during this period of pore expansion (40). Problematically, if nonvesicular lipid transport does shuttle curvature-supporting lipids from

the reticulum to the plasma membrane, then they must be redistributed from the cytoplasmic leaflet adjacent to the reticulum to the extracellular leaflet facing the junction cleft (Fig. 10C). A variety of lipid flippase and scramblase genes also show peak transcriptional activity early during conjugation in *Tetrahymena*, e.g., TTHERM_00123720 and TTHERM_00264820 (40; N. Stover, personal communication).

These conjectures provide an attractive model for how specialized, nonlamellar lipids might first be delivered to the cytoplasmic face of the pore membrane and then translocate to the extracellular face as cells remodel the membrane to support the growing regions of tight curvature associated with the membrane pores. Such a model is consistent with the "timing" considerations raised by Kurczy et al. (38). These investigators noted that pore formation precedes change in lipid composition within the exchange junction, a view congruent with our observations of the transjunction reticulum becoming established after membrane fusion and pore formation are already complete.

There is one final possibility: studies have implicated calcium signaling as essential during early stages of pair formation in ciliates (41). The ER is a well-known reservoir for calcium ions. Having an endoplasmic store of calcium deployed at the nuclear exchange junction could help to regulate local calcium signals during cortical remodeling.

Extracellular microvesicles at the exchange junction. As membrane pores become established, the process of membrane protrusion seems to continue in close proximity to the initial pores (though without the subsequent fusion). The result is a proliferation of extracellular tubules and vesicles (EMVs) that collect within small pockets of the junction cleft. These pockets swell into blisters of extracellular space that we refer to as junction lumens. Our impression is that these vesicle-filled pockets are subsequently internalized through a process of reclamation resulting in structures that resemble multivesicular bodies (objects that are abundant within the junction cytoplasm at this time). These EMV-filled vacuoles are also observed being encompassed by double-walled autophagosomes, suggesting that they are destined for cytoplasmic degradation. This process could represent a unique form of membrane removal that operates in support of pore expansion.

The production of EMVs within the exchange junction lumen may simply represent a form of membrane extraction or downregulation of surface components. Yet the literature suggests that such structures can serve other purposes as well. There is a growing body of evidence suggesting that shed microvesicles can carry specific proteins or even microRNA (miRNA) from one cell to another, thereby effecting changes in gene expression or physiological responses in the recipient (19, 42). The phenomena that we describe could fulfill both these functions. These rather unique EMVs may indeed remove membrane components from the expanding exchange junction pores, thereby facilitating the process of pore expansion, but at the time that pore expansion is under way (2 to 4 h into mating), there is massive expression of microRNA from the premeiotic, germ line micronuclei in mating cells (43, 44). This process has been implicated in an miRNA-mediated mechanism of genome remodeling that involves precise DNA excision. It has also been noted that there is some form of communication between mating cells affecting DNA excision, even when no genetic material is exchanged (45). It is intriguing to speculate that in *Tetrahymena*, shed microvesicles may somehow be involved in cell-cell signaling as conjugation is initiated. It is significant that constitutive secretion involving some form of extracellular microvesicles has been demonstrated in *T. thermophila* (46).

A model of membrane dynamics at the developing nuclear exchange junction. We offer the following model summarizing membrane dynamics associated with formation of the nuclear exchange junction during early stages (1 to 4 h) of mating in *Tetrahymena thermophila* (Fig. 11). To begin with, we propose a localized thinning of the junction scaffold, an electron-dense cytoskeletal mesh closely applied to both sides of the junction membrane (Fig. 11A and B). Unilateral membrane deformations create "male" protrusions at hundreds of sites initiated independently from both mating partners (Fig. 11C). Membrane fusion between the tips of these 50-nm-wide protrusions and the plasma membrane of the mating partner create sites of cytoplasmic continuity (Fig. 11D). Following pore formation, the process of membrane protrusion (without concomitant fusion) continues, creat-
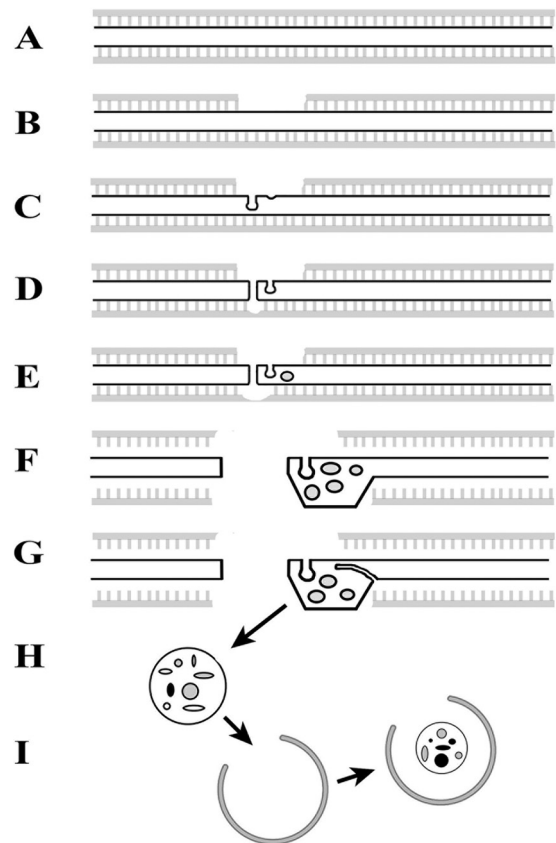
FIG 11 Model illustrating pore formation. Faint gray lines represent the junction "scaffold" with struts connecting it to the plasma membranes (thin black lines). (A) Membranes during cell adhesion (0 to 1.5 h). (B) Clearing of scaffold over future pore site. (C) Evagination of membrane protuberances into extracellular space of the junction cleft. (D) Fusion of one protuberance creating a cytoplasmic bridge between cells. (E and F) Continued evagination into the vicinity of the pore excavates membrane supporting pore expansion and produces extracellular microvesicles within junction lumens. (G) Membrane folds delimit extracellular space, including microvesicles within a vacuole in a form of bulk endocytosis. (H) A membrane-bound vacuole with microvesicle contents (MVB-like in appearance) becomes internalized within the cell's cytoplasm, where it enters neighboring autophagosomes (I).

ing populations of extracellular microvesicles (Fig. 11E and F). This process results in extraction of membrane material from the walls of an adjacent pore and accumulation of extracellular, membrane-bound vesicles trapped within growing pockets of extracellular space, the so-called junction lumens (Fig. 11F). We propose that this process may excavate membrane from the margins of adjacent pores, allowing for their expansion. During a second type of membrane deformation, a reclamation fold envelops these extracellular vesicles and tubules within a limiting membrane, partitioning them into the cytoplasm (Fig. 11G and H). They now resemble multivesicular bodies (MVBs), with an outer limiting membrane enveloping a collection of membrane-bound vesicles or tubules (Fig. 11H). During these membrane-remodeling events, the anterior cytoplasm fills with double-membrane cups and vacuoles fitting the description of autophagosomes. We observed such autophagosome-like compartments enclosing MVB-like structures, and in one case, we captured a structure resembling an autophagosome forming directly around a junction lumen in the process of reclamation (Fig. 6D to F and 11I). Taken

together, these structures and processes constitute a possible mechanism of pore formation and pore expansion during the early stages of conjugation. During pore expansion, a novel membrane system (the transjunction reticulum) develops and infiltrates the developing pores. We further propose that this membrane system could represent a means of reconstituting phospholipid species that populate the exchange junction, helping to restructure it from a pair of laminate membrane sheets into a reticulum of tightly curved tubules. (We do not rule out other possible functions such as a role in calcium signaling or membrane extraction, though the latter seems unlikely.)

REFERENCES

1. **Wolfe J.** 1982. The conjugation junction of Tetrahymena: its structure and development. J Morphol **172**:159–178.
2. **Orias JD, Hamilton EP, Orias E.** 1983. A microtubular meshwork associated with gametic pronuclear transfer across a cell-cell junction. Science **222**:181–184.
3. **Suganuma Y, Shimode C, Yamamoto H.** 1984. Conjugation in Tetrahymena: formation of a special junction area for conjugation during the co-stimulation period. J Electron Microsc (Tokyo) **33**:10–18.
4. **Cole ES.** 2006. The Tetrahymena conjugation junction, p 39–62. In Baluska F, Volkmann D, Barlow PW (ed), Cell-cell channels. Springer, New York, NY.
5. **Bruns PJ, Brussard TB.** 1974. Pair formation in Tetrahymena pyriformis, an inducible developmental system. J Exp Zool **188**:337–344.
6. **Wellnitz WR, Bruns PJ.** 1979. The pre-pairing events in Tetrahymena thermophila: analysis of blocks imposed by high concentrations of Tris-Cl. Exp Cell Res **119**:175–180.
7. **Nanney DL, Caughey PA.** 1953. Mating type determination in Tetrahymena pyriformis. Proc Natl Acad Sci U S A **39**:1057–1063.
8. **Cervantes MD, Hamilton EP, Xiong J, Lawson MJ, Yuan D, Hadjithomas M, Miao W, Orias E.** 2013. Selecting one of several mating types through gene segment joining and deletion in Tetrahymena thermophila. PLoS Biol **11**(3):e1001518. http://dx.doi.org/10.1371/journal.pbio.1001518.
9. **Bruns PJ, Palestine RF.** 1975. Costimulation in Tetrahymena pyriformis: a developmental interaction between specially prepared cells. Dev Biol **42**:75–83.
10. **Finley MJ, Bruns PJ.** 1980. Costimulation in Tetrahymena. II A nonspecific response to heterotypic cell-cell interactions Dev Biol **79**:81–94.
11. **Orias E, Hamilton EP, Orias JD.** 2000. Tetrahymena as a laboratory organism: useful strains, cell culture, and cell line maintenance. Methods Cell Biol **62**:189–211.
12. **Reynolds ES.** 1963. The use of lead citrate at high pH as an electron-opaque stain in electron microscopy. J Cell Biol **17**:208–212.
13. **Meehl JB, Giddings, TH, Jr, Winey M.** 2009. High pressure freezing, electron microscopy, and immuno-electron microscopy of Tetrahymena thermophila basal bodies, p 227–241. In Gavin RH (ed), Cytoskeleton methods and protocols. Humana Press Inc, Totowa, NJ.
14. **Giddings TH, Meehl JB, Pearson CG, Winey M.** 2010. Electron tomography and immuno-labeling of Tetrahymena thermophila basal bodies. Methods Cell Biol **96**:117–141. http://dx.doi.org/10.1016/S0091-679X(10)96006-8.
15. **Mastronarde DN.** 2005. Automated electron microscope tomography using robust prediction of specimen movements. J Struct Biol **152**:36–51. http://dx.doi.org/10.1016/j.jsb.2005.07.007.
16. **Mastronarde DN.** 1997. Dual-axis tomography: an approach with alignment methods that preserve resolution. J Struct Biol **120**:343–352.
17. **Kremer JR, Mastronarde DN, McIntosh JR.** 1996. Computer visualization of three-dimensional image data using IMOD. J Struct Biol **116**:71–76.
18. **Rutter GA, Tsuboi T.** 2004. Kiss and run exocytosis of dense core secretory vesicles. NeuroReport **15**:79–81.
19. **Cocucci E, Racchetti G, Meldolesi J.** 2009. Shedding microvesicles: artefacts no more. Trends Cell Biol **19**:43–51. http://dx.doi.org/10.1016/j.tcb.2008.11.003.
20. **Raposo G, Stoorvogel W.** 2013. Extracellular vesicles: exosomes, microvesicles, and friends. J Cell Biol **200**:373–383. http://dx.doi.org/10.1083/jcb.201211138.
21. **Lee TH, D'Asti E, Magnus N, Al-Nedawi K, Meehan B, Rak J.** 2011. Microvesicles as mediators of intercellular communication in cancer—the emerging science of cellular 'debris.' Semin Immunopathol **33**:455–467. http://dx.doi.org/10.1007/s00281-011-0250-3.
22. **Nilsson JR.** 1984. On starvation-induced autophagy in Tetrahymena. Carlsberg Res Commun **49**:323–340.
23. **Endoh H, Kobayashi T.** 2006. Death harmony played by nucleus and mitochondria: nuclear apoptosis during conjugation of tetrahymena. Autophagy **2**:129–131. http://dx.doi.org/10.4161/auto.2.2.2368.
24. **Akematsu T, Pearlman RE, Endoh H.** 2010. Gigantic macroautophagy in programmed nuclear death of Tetrahymena thermophila. Autophagy **6**:901–911. http://dx.doi.org/10.4161/auto.6.7.13287.
25. **Kobayashi T, Endoh H.** 2006. Tetrahymena nuclear apoptosis and a role of mitochondrial endonuclease. Zool Sci (Tokyo) **23**:1181.
26. **Kitamura A, Sugai T, Kitamura Y.** 1986. Homotypic pair formation during conjugation in Tetrahymena thermophila. J Cell Sci **82**:223–234.
27. **Wolfe, J, Feng S** 1988. Concanavalin A receptor "tipping" in Tetrahymena and its relationship to cell adhesion during conjugation. Development **102**:699–708.
28. **Pagliaro L, Wolfe J.** 1989. Concanavalin A inhibits mating type recognition in Tetrahymena. Exp Cell Res **181**:574–578.
29. **Frisch A, Levkovitz H, Loyter A.** 1977. Inhibition of conjugation in Tetrahymena pyriformis by concanavalin A. Binding of concanavalin A to material secreted during starvation and to washed cells. Exp Cell Res **106**:293–301.
30. **Goodenough, UW, Weiss RL.** 1975. Gametic differentiation in Chlamydomonas reinhardtii. III. Cell wall lysis and microfilament-associated mating structure activation in wild-type and mutant strains. J Cell Biol **67**:623–637.
31. **Mori T, Kuroiwa H, Higashiyama T, Kuroiwa T.** 2006. GENERATIVE CELL SPECIFIC 1 is essential for angiosperm fertilization. Nat Cell Biol **8**:64–71. http://dx.doi.org/10.1038/ncb1345.
32. **Cole ES, Cassidy-Hanley D, Pinello JF, Zeng H, Hseuh M, Kolbin D, Ozzello C, Giddings T, Jr, Winey M, Clark TG.** 2014. Function of the male-gamete-specific fusion protein HAP2 in a seven-sexed ciliate. Curr Biol **24**:2168–2173. http://dx.doi.org/10.1016/j.cub.2014.07.064.
33. **Maule AJ.** 2008. Plasmodesmata: structure, function and biogenesis. Curr Opin Plant Biol **11**:680–686. http://dx.doi.org/10.1016/j.pbi.2008.08.002.
34. **Tilsner J, Amari K, Torrance L.** 2011. Plasmodesmata viewed as specialised membrane adhesion sites. Protoplasma **248**:39–60. http://dx.doi.org/10.1007/s00709-010-0217-6.
35. **Paul LK, Rinne PLH, Van der Schoot C.** 2014. Refurbishing the plasmodesmal chamber: a role for lipid bodies? Frontiers Plant Sci **5**:40. http://dx.doi.org/10.3389/fpls.2014.00040.
36. **Snapp EL, Iida T, Frescas D, Lippincott-Schwartz J, Lilly MA.** 2004. The fusome mediates intercellular endoplasmic reticulum connectivity in Drosophila ovarian cysts. Mol Biol Cell **15**:4512–4521. http://dx.doi.org/10.1091/mbc.E04-06-0475.
37. **Ostrowski SG, Van Bell CT, Winograd N, Ewing AG.** 2004. Mass spectrometric imaging of highly curved membranes during tetrahymena mating. Science **305**:71–73. http://dx.doi.org/10.1126/science.1099791.
38. **Kurczy ME, Piehowski PD, Van Bell CT, Heien ML, Winograd N, Ewing AG.** 2010. Mass spectrometry imaging of mating Tetrahymena show that changes in cell morphology regulate lipid domain formation. Proc Natl Acad Sci U S A **107**:2751–2756. http://dx.doi.org/10.1073/pnas.0908101107.
39. **Lev S.** 2010. Non-vesicular lipid transport by lipid-transfer proteins and

beyond. Nat Rev Mol Cell Biol **11:**739–750. http://dx.doi.org/10.1038/nrm2971.

40. **Miao W, Xiong J, Bowen J, Wang W, Liu Y, Braguinets O, Grigull J, Pearlman RE, Orias E, Gorovsky MA.** 2009. Microarray analyses of gene expression during the Tetrahymena thermophila life cycle. PLoS One **4**(2):e4429. http://dx.doi.org/10.1371/journal.pone.0004429.

41. **Cronkite DL.** 1976. A role of calcium ions in chemical induction of mating in Paramecium tetraurelia. J Protozool **23:**431–433.

42. **Hunter MP, Ismail N, Zhang X, Aguda BD, Lee EJ, Yu L, Xiao T, Schafer J, Lee ML, Schmittgen TD, Nana-Sinkam SP, Jarjoura D, Marsh CB.** 2008. Detection of microRNA expression in human peripheral blood microvesicles. PLoS Biol **3**(11):e3694. http://dx.doi.org/10.1371/journal.pone.0003694.

43. **Chalker DL, Fuller P, Yao MC.** 2005. Communication between parental and developing genomes during tetrahymena nuclear differentiation is likely mediated by homologous RNAs. Genetics **169:**149–160. http://dx.doi.org/10.1534/genetics.104.032300.

44. **Mochizuki K, Gorovsky MA.** 2004. Small RNAs in genome rearrangement in Tetrahymena. Curr Opin Genet Dev **14:**181–187. http://dx.doi.org/10.1016/j.gde.2004.01.004.

45. **Chalker DL.** 2005. Genome rearrangements: Mother knows best! Curr Biol **15**(20)**:**R827–R829. http://dx.doi.org/10.1016/j.cub.2005.09.045.

46. **Madinger CL, Collins K, Fields LG, Taron CH, Benner JS.** 2010. Constitutive secretion in Tetrahymena thermophila. Eukaryot Cell **9:**674–681. http://dx.doi.org/10.1128/EC.00024-10.